Effect of Boehmite Crystallite Size and Steaming on Alumina Properties

M. L. Guzmán-Castillo,[†,*] X. Bokhimi,[†,‡] A. Toledo-Antonio,[†] J. Salmones-Blásquez,[†] and F. Hernández-Beltrán[†]

Instituto Mexicano del Petróleo, Eje Central L. Cárdenas 152, C.P. 07730 México D.F., México, and Institute of Physics, The National University of Mexico (UNAM), A. P. 20-364, C.P. 01000 México D.F., México

Received: March 17, 2000; In Final Form: September 16, 2000

Boehmite and pseudoboehmite were studied in order to find the effect of their individual properties upon the properties of transitional alumina and α-Al_2O_3 produced thereof; the influence of steaming on these properties was also considered. Samples were characterized by X-ray powder diffraction, crystalline structure refinement, scanning electron microscopy, thermoanalysis, and nitrogen adsorption. Boehmite and pseudoboehmite had the same crystalline structure but different crystallite dimensions. Differences between lattice parameters (only 0.0052 nm along the *b* axis) are so small that the assumption of many authors that pseudoboehmite has intercalated water in its crystalline structure cannot be supported. Small crystallites with larger active areas, increased by crystal faces perpendicular to (020) planes, explain the larger amounts of desorbed water that pseudoboehmite exhibits compared to boehmite while drying. The hydrogen-bond length in boehmite depends on the crystallite size and determines the temperature where transformation into transitional alumina takes place. The boehmite crystallite size also defined pore size and distribution in transitional aluminas as well as their grain and crystallite size. Since the transformation of the transitional alumina into α-Al_2O_3 depends on hydroxyls diffusion, the corresponding temperature is higher for the transitional alumina with a larger grain size. Steaming promoted crystal growth, because water molecules favored migration of aluminum atoms. Nitrogen adsorption−desorption isotherms of transitional aluminas derived from pseudoboehmite exhibited hysteresis loops corresponding to less ordered structures associated with swelling of platelets during desorption of nitrogen molecules. Consequences on the properties of transitional aluminas used as cracking catalysts were inferred. As texture and acidity evolve in opposite directions, there is a need for controlling them independently.

Introduction

Transitional aluminas are widely used as catalysts and catalyst supports in several processes related to petroleum refining and the petrochemical and chemical industries.[1−4] The extended usage of transitional aluminas in catalysis is explained by their particular properties that combine high specific areas, high thermal stability, and mechanical strength and by the fact that their acid−base properties and porosity may be varied by a relatively large extent.

Application of transitional aluminas is of special interest in fluid catalytic cracking (FCC),[5−13] which is one of the most important oil refining processes worldwide. The active component of a fluid cracking catalyst is a faujasite "Y" zeolite supported on a matrix that can have different compositions. The fluid cracking catalysts which contain transitional aluminas exhibit higher matrix activity compared to catalysts containing untreated clay or large amounts of silica.

One of the current approaches in FCC heavy and reside feeds processing is to design catalysts with moderate zeolite contents and a significant nonzeolitic large pore activity.[6] Both, meso- and macropores coupled to a relatively high acidity are necessary for efficient cracking of heavy feeds.[11] Those types of feeds, however, are highly contaminated with metals (nickel and vanadium are the most abundant), which disperse on the matrix and act as dehydrogenating centers, increasing gas and coke yields that constrains unit operation. Therefore, besides bottoms upgrading and relative low coke and gas production capabilities, alumina-based matrixes should also feature high metals tolerance in order to minimize the deleterious contaminant selectivity. EXAFS and fixed fluid bed testing studies carried out on nickel-contaminated FCC catalysts suggest that matrices promoting formation of nickel aluminate exhibit superior metals tolerance.[12]

Since high temperatures and steam atmospheres are prevailing conditions in the operating cycles in FCC units, hydrothermal stability is also needed for a robust alumina matrix, specially in reside cracking operations.[13]

The properties that govern the performance of aluminas as cracking catalyst are interdependent and evolve with opposite trends. It is well-known that the higher the specific surface, the higher the acidity, the lesser the stability, and the lesser the pore size. Therefore it becomes of paramount importance to have a better understanding of the origin of changes in properties of alumina induced by thermal and hydrothermal conditions and how the properties of precursors are concerned. Although a great number of studies have been published through the years on these subjects, a full picture of the atomic structure of boehmites is still missing. A better comprehension of the boehmite structure and the mechanism that controls its transformation through transitional alumina will help to control catalytic cracking properties.

This work dealt with the study of structural aspects of aluminas and their precursors. Fine details of the structure of boehmite and pseudoboehmite were studied with the aim of

[†] Instituto Mexicano del Petróleo.
[‡] The National University of Mexico.

10.1021/jp001024v CCC: $20.00
Published on Web 02/22/2001

understanding differences between the transitional aluminas produced thereof. The interdependency among porosity, crystal size, and structure at the atomic level was addressed. The effects of steaming upon these properties were also studied.

Experimental Section

Sample Preparation. Powdered samples of aluminum oxyhydroxide, namely pseudoboehmite (PSB) and boehmite (BOE), were studied. BOE was kindly provided by Grace-Davison, whereas PSB was obtained from Condea (Catapal). Samples were annealed at 788 °C during 4 h in static air (PSB-C, and BOE-C) or steamed (PSB-S, and BOE-S). Steaming took place with 100% steam using 20 g of powdered material in a vertical quartz tubular reactor where distilled liquid water was vaporized and entered from the bottom at 0.2 mL min^{-1}.

Characterization Techniques. X-ray diffraction measurements were performed at room temperature with Cu Kα radiation in a Bruker Advance D-8 diffractometer having $\theta-\theta$ configuration and a graphite secondary-beam monochromator. Sample powders were packed in a glass holder. Diffraction intensity was measured by step scanning in the 2θ range between 10 and 110°, with a 2θ step of 0.02° for 8 s per point. Crystalline structures were refined with the Rietveld technique by using DBWS-9411[14] and FULLPROF-V3.5d[15] programs; peak profiles were modeled with a pseudo-Voigt function[16] that depends on average crystallite size.[17] Standard deviations, which show the last figure variations of a number, are given in parentheses. When these deviations correspond to Rietveld refined parameters, their values are not estimates of the probable error in the analysis as a whole but only of minimum possible probable errors based on their normal distribution.[18]

Nitrogen adsorption isotherms were obtained at −196 °C with a Micromeritics ASAP-2100 apparatus. The specific area of solids was calculated by the multipoint BET method. The pore size distribution and shape are closely related to the hysteresis loop classified by IUAPAC,[19] BET,[20] or BDDT.[21] The analysis of the adsorption−desorption isotherms was complemented following criteria on the inspection of the hysteresis loop shape based on the so-called descending boundary curve (DBC).[22]

Weight loss and temperatures associated with phase transformation were determined by thermogravimetry (TG) and differential thermal analysis (DTA) using a Perkin-Elmer TG-7 and a Perkin-Elmer 1700 apparatus, respectively. The sample (10 mg) was heated in flowing dried air (20 mL min^{-1}) from room temperature up to 1000 °C at 10 °C min^{-1}; DTA was carried out using platinum crucibles and α-alumina as reference.

Micrographs of fresh, calcined, and steamed samples were obtained using a JEOL 35 CF scanning electron microscope (SEM).

Results and Discussion

Crystallography and Crystallite Morphology. X-ray diffraction patterns of fresh, calcined, and steamed samples are presented in Figures 1 and 2. Boehmite and pseudoboehmite samples contained only one phase (Figures 3 and 4), which was refined with an orthorhombic unit cell having the symmetry described by the space group *Cmcm* and atoms in the positions given in Tables 1 and 2. Atom positions for BOE and PSB were very similar, differing only in the third decimal digit. The lattice parameters in both samples were also similar (Table 3). Only a difference of 0.0052 nm was found along the *b* axis. The most open planes of the structure, which correspond to the (020) reflection (Figure 1), had a difference of only 0.0026 nm, in which no atom can be intercalated. This means that the

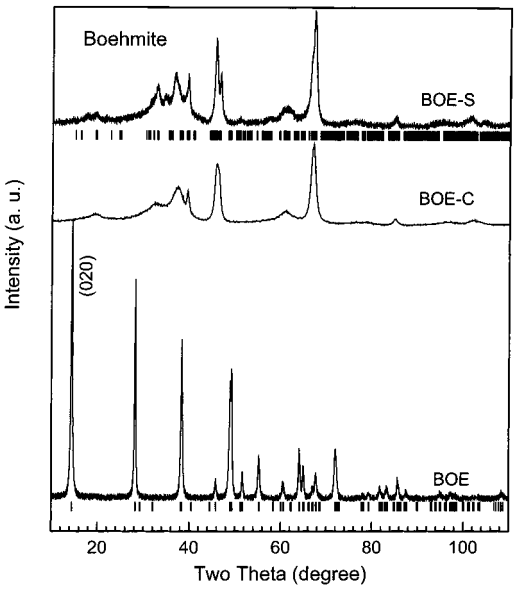

Figure 1. X-ray diffraction patterns of the samples derived from the boehmite with a crystallite thickness of 26.1(5) nm. The tick marks under the pattern of BOE-C and BOE correspond to θ-alumina and boehmite, respectively.

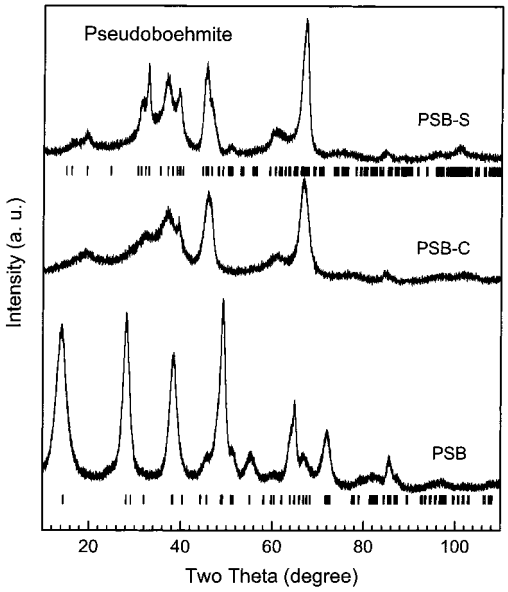

Figure 2. X-ray diffraction patterns of the samples derived from the boehmite with a crystallite of 3.42(4) nm. The tick marks under the pattern of PSB-C and PSB correspond to θ-alumina and boehmite, respectively.

difference between boehmite and pseudoboehmite cannot be produced by molecules of water intercalated in (020) planes, as has been assumed in the literature.[23,24]

Crystallite morphology in both boehmite samples was anisotropic. Crystallites were thin platelets with their shortest dimension along the *b* axis. This anisotropy produced diffraction peak widths that depended on Miller indices. Since the thinnest part of the crystallite was along the *b* axis, the broadest diffraction peaks were those produced by the planes perpendicular to this axis, i.e., those corresponding to (0*k*0) reflections. FULLPROF code[15] can model this effect, allowing us to refine correctly the crystalline structure. From refinements a crystallite thickness of 26.1(5) nm for BOE and 3.32(4) nm for PSB (Table 3) was obtained.

Figures 3 and 4 show their corresponding Rietveld refinement plots. Although experimental data fit was good, we tried to

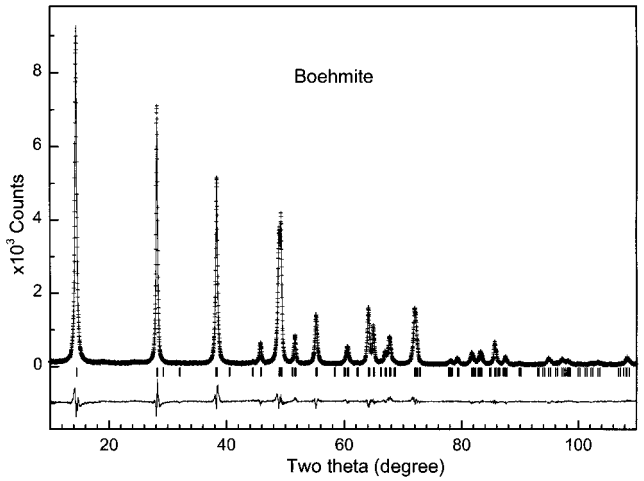

Figure 3. Rietveld refinement plot of BOE (Rwp = 0.14). Experimental data are indicated with cross marks, and the calculated one and the difference between them, with continuous lines. Tick marks correspond to boehmite (R_{Bragg} = 0.045).

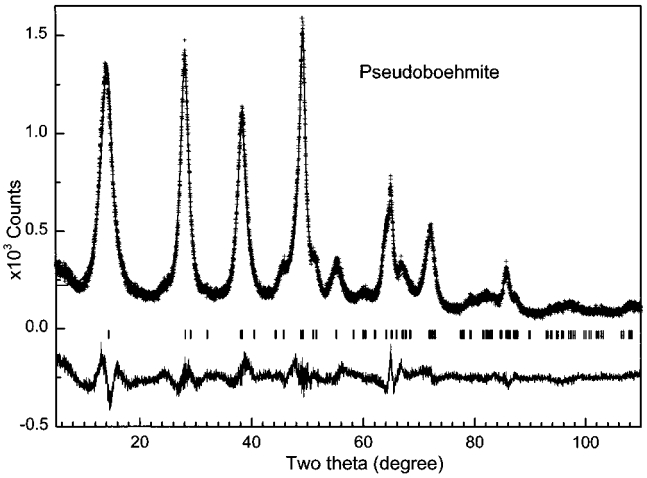

Figure 4. Rietveld refinement plot of PSB (Rwp = 0.13). Experimental data are indicated with cross marks, and the calculated one and the difference between them, with continuous lines. Tick marks correspond to boehmite (R_{Bragg} = 0.031).

TABLE 1: Boehmite, Space Group *Cmcm*: Atom Fractional Coordinates[a]

atom	**site**	x	***y***	z
Al	4c	0.0	y_{Al}	0.25
O	4c	0.0	y_{O}	0.25
O_H	4c	0.0	y_{OH}	0.25

[a] Since hydrogen X-ray diffraction is negligible, it was not considered. O_H is the atom position of the oxygen atoms associated with hydroxyls.

TABLE 2: Atom Fractional Coordinates *y* for the Different Atoms

sample	y_{Al}	y_{O}	y_{OH}
BOE	−0.3180(2)	0.2907(2)	0.0784(2)
PSB	−0.3199(3)	0.2979(4)	0.0779(3)

improve it by modeling microstrains. FULLPROF code[15] has several models for this microstrain, some of them related to crystalline unit cells with orthorhombic symmetry,[25] which corresponds to the symmetry actually observed in our samples. None of these models, however, gave rise to a better fit of the experimental data; on the contrary, when they were applied, the temperature factors were negative, which is meaningless.

TABLE 3: Lattice Parameters and Average Crystallite Thickness

sample	*a* (nm)	*b* (nm)	*c* (nm)	*d*(020) (nm)
BOE	0.28683(1)	1.2221(6)	0.36958(1)	26.1(5)
PSB	0.28679(5)	1.2273(5)	0.37021(7)	3.32(4)

TABLE 4: Lattice Parameters and Average Crystallite Size of the Transitional Aluminas produced from boehmite

sample	*a* (nm)	*b* (nm)	*c* (nm)	β (deg)	*d* (nm)
BOE-C	1.215(2)	0.2799(4)	0.5576(8)	102.9(1)	6.6(2)
BOE-S	1.2030(8)	0.2817(2)	0.5574(4)	103.21(6)	7.0(2)
PSB-C	1.218(1)	0.2789(3)	0.5547(5)	102.99(7)	3.52(6)
PSB-S	1.1979(6)	0.2852(1)	0.5575(3)	103.14(6)	6.03(8)

Therefore, microstrain effects were excluded from the refinement of boehmite's crystalline structure.

The above results suggest that, from the crystallographic point of view, the only notable difference between boehmite and pseudoboehmite is the crystallite size. For that reason, instead of referring to boehmite and pseudoboehmite as two different phases, from here on we will refer to them as boehmite, but with different crystallite size which reflects the real properties of this system (sample designations were kept for clearness). This conclusion will certainly conflict with the accepted and traditional way of distinguishing these materials; however, the evidence obtained in the present work leads us to conclude that they correspond to the same crystalline phase.

As will be evident, the transitional alumina properties depend on the crystallite size of the precursor to a great extent. Therefore, for practical meaning, it becomes of great interest to characterize it in a relatively simple way. Boehmite crystallites are thin plates whose smallest dimension is along the *b* axis. By consequence, the (020) X-ray reflection—the one at the lowest 2θ angle (Figure 1) that is strong and not superimposed with other reflections (Figures 3 and 4)—can be used to characterize it. The full width at half-maximum (fwhm) of this peak is related to the average crystallite thickness and thus might be used to characterize this dimension. This will only require the measurement of the diffraction pattern in the 2θ region between 9 and 19°, which might be easily implemented from a practical standpoint.

The crystalline structure of the transitional aluminas in samples BOE-C, BOE-S, PSB-C, and PSB-S was modeled with the monoclinic unit cell reported for θ-alumina,[26] which is derived from the spinel structure. The atom positions in the monoclinic unit cell have the symmetry described by the space group *C*2/*m*. The residue obtained after the refinement with the above unit cell was 10% smaller than with the nondeformed cubic unit cell having a spinel structure. Table 4 gives the lattice cell parameters and the average crystallite sizes obtained after refinement.

Aluminas derived from BOE had larger crystallites than those derived from PSB (Table 4). Differences were more pronounced when alumina was prepared in air (Table 4). For example, the alumina derived from the boehmite (BOE) with the thick crystallite (Figure 1), 26.1(5) nm, had an average crystallite size of 6.6(2) nm, while the one derived from the boehmite (PSB) with thin crystallites (Figure 2), 3.32(4) nm, had an average crystallite size of 3.52(6) nm.

Boehmite's crystallite dimensions also had an effect upon the transformation rate of the corresponding transitional alumina into the nonhydroxylated α-alumina (Figure 5). For instance, when transitional aluminas were annealed for 20 h at 1100 °C, samples derived from PSB were completely transformed into α-alumina, whereas those derived from BOE transformed only

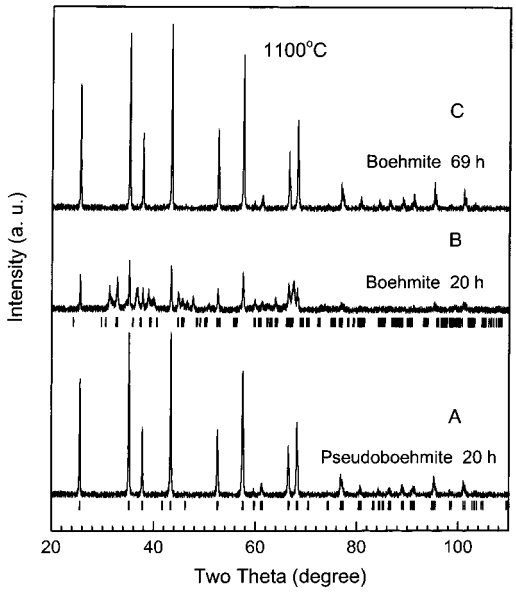

Figure 5. X-ray diffraction patterns of BOE and PSB after calcining at 1100 °C: (A) PSB calcined for 20 h, (B) BOE calcined for 20 h, (C) BOE calcined for 69 h. The tick marks under the boehmite pattern correspond to the monoclinic phase; those under the pattern of the pseudoboehmite correspond to α-alumina.

SCHEME 1: Pseudomorphic Evolution of Boehmite Crystallites into Those of Transitional Alumina and These into α-Al_2O_3

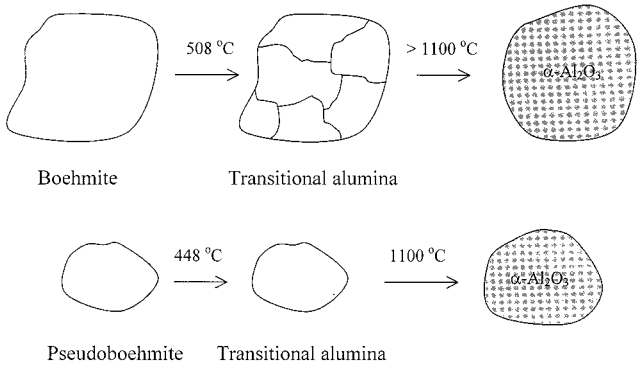

partially into α-alumina. Transformation was completed only after 69 h at this temperature.

The observed crystallite size dependence of transitional aluminas transformation (into α-alumina) can be explained in terms of the pseudomorphic character of the process.[27,28] A boehmite crystallite is transformed into several alumina crystallites, forming a single grain with the dimensions of the original boehmite crystallite (Scheme 1). Therefore, BOE-C exhibited a larger crystal grain compared to PSB-C. Transformation of transitional alumina into α-alumina is determined by the dehydroxylation process where hydroxyl diffusion is a controlling step below 1100 °C. Since the path hydroxyls should go through is shorter for small grains (Scheme 1), the complete transformation of these grains into α-alumina occurs faster than for large grains, where hydroxyls takes longer to leave (Figure 5C). This explains the fact that DTA or any other heating treatment at fixed heating rate or fixed temperature show that transitional aluminas with large crystallites require either high temperatures or long times before a complete transformation into α-Al_2O_3 (Figure 5B,C) takes place.[23]

Water Desorption and Phase Transformation. Boehmite samples exhibited three weight loss stages as a function of temperature. The first stage was observed from room temperature up to 90 °C for BOE and up to 120 °C for PSB (Figure 6 and Table 5). This stage corresponded to the desorption of water molecules adsorbed on crystallites surface. The weight loss in PSB was comparatively higher due to its smaller crystallite size and thus higher surface areas available for water adsorption.

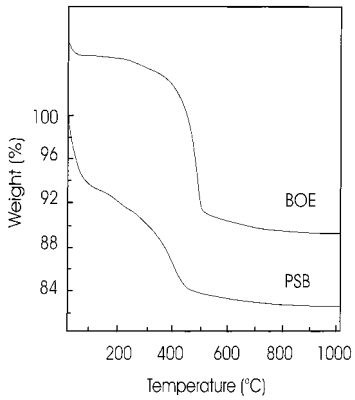

Figure 6. TG curves of BOE and PSB.

TABLE 5: Weight Loss Stages (weight %) by TGA

sample	stage 1	stage 2	stage 3
BOE	1.281	14.44	1.42
PSB	10.63	14.76	1.45

The above argument seems obvious but can be detailed further from structural considerations. Boehmite crystal structure has double layers—parallel to the (020) planes—of octahedra sharing edges along the *a* axis and vertexes along the *c* axis, with an aluminum atom near their center and two hydroxyls and four oxygen atoms in their vertexes.[29] The interaction within a double layer is strong, but between double layers it is weak (via hydrogen bonds). Therefore, a boehmite crystallite ends in the interface between two double layers, thus producing surfaces that are full of hydroxyls. The crystallite surfaces perpendicular to double layers have oxygen atoms in low coordination. These oxygen atoms can easily react with hydroxyls and hydrogen ions from their environment, thus allowing these surfaces to get fully covered with hydroxyls. For small crystallite size, the number of these low coordination oxygen sites increases, thus leading more water molecules to be adsorbed compared to larger crystallite sizes.

A second weight loss stage showed by TG analysis was found between 90 and 550 °C for BOE and between 120 and 460 °C for PSB. This stage corresponded to the transition, via an endothermic reaction (Figure 7), into the corresponding transitional alumina. The third weight loss stage, which was not so clearly defined as the two precedent, corresponded with a continuous and gradual loss of residual hydroxyls, which is characteristic of transitional aluminas.[23,30]

The temperatures associated with transformation into transitional alumina depended on boehmite's crystallite dimensions (Tables 3 and 6). According to DTA, this temperature was 448 °C for boehmite (PSB) with small crystallites and 508 °C for boehmite (BOE) with large crystallites. This difference is related to the hydrogen-bond strength between double layers (Table 6).[31] Although, for the present study the difference between hydrogen-bond lengths was only 0.0012 nm, a systematic study[29] showed that atom bonds in boehmite depend on the crystallite size and that the transition into γ-alumina is related to the hydrogen bond.[31]

Crystal Aggregation. When transitional aluminas were subjected to steaming (samples BOE-S and PSB-S), they

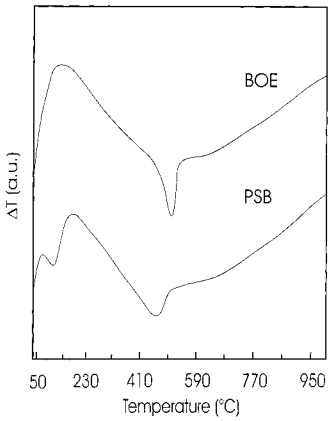

Figure 7. DTA curves of BOE and PSB.

TABLE 6: Transition Temperature of Boehmite into γ-alumina and Some Characteristic Atom Bond Lengths[a]

sample	T (°C)	$d_{OH\text{-}O}$ (nm)	d_{Al-OH} (nm)	d_{Al-O_a} (nm)	d_{Al-O_c} (nm)
BOE	448	0.2678(1)	0.1907(1)	0.1952(1)	0.1878(1)
PSB	508	0.2800(1)	0.1905(1)	0.1990(1)	0.1879(1)

[a] Hydrogen-bond length = $d_{O-H\text{-}O}$. Bond lengths of the interaction of aluminum with oxygen atoms (which determine unit cell dimension along lattices parameters) = d_{Al-O_a} along the *a* axis, d_{Al-OH} along the *b* axis, and d_{Al-O_c} along the *c* axis.

produced samples with larger crystallites (Table 4). It seems that water molecules favored aluminum transport for crystal growth, which explains the absence of small crystal aggregates in the steamed samples (Figures 8A and 9A). BOE samples were homogeneously formed by spherical crystal aggregates with diameters between 5 and 50 μm (Figure 10A) and composed by oriented platelet-like crystals. In contrast, PSB samples did not show a specific grain form (Figure 10B). The grain morphology in BOE did not change upon transformation into transitional alumina (Figure 8), which agrees with the pseudomorphic character of this process, as has been already discussed. A similar but more pronounced effect was observed for PSB (Figure 9). Under steaming conditions, the initial irregular grain aggregates were transformed into nonspherical grains with similar dimensions. Thus the effect of annealing in air was only to disaggregate the initial boehmite grains (Figures 8B and 9B).

Pore Size Distribution. Analysis of the hysteresis loop shape by using the descending boundary curve (DBC)[20−22] technique provides information about pore blocking and pore structure rigidity in alumina samples. The hysteresis loop shape of aluminas derived from BOE (Figure 11) corresponds to structures of medium strength without pore blockage.[22] Therefore, steaming had only a weak effect on pore size distribution (Figure 12). Aluminas from BOE had mesopores with diameters between 10 and 100 nm, though diameters between 50 and 100 nm dominated (Figure 12).

The initial slopping character on the descending boundary curves observed for PSB-C and PSB-S (Figure 13) reflects the porous structure shrinkage caused by stress change of the condensate during depressurization. This is due to swelling of parallel grain plates by adsorbed nitrogen,[22] because the structures in these samples were less rigid than those found for aluminas derived from BOE. The plateau of the descending boundary curve of PSB-C and PSB-S indicates an appreciable pore blockage. Moreover, the hysteresis loop type would suggest that a mixture between ink-bottle and interstitial pores between aggregates according to De Boer and Lippens[32] classification

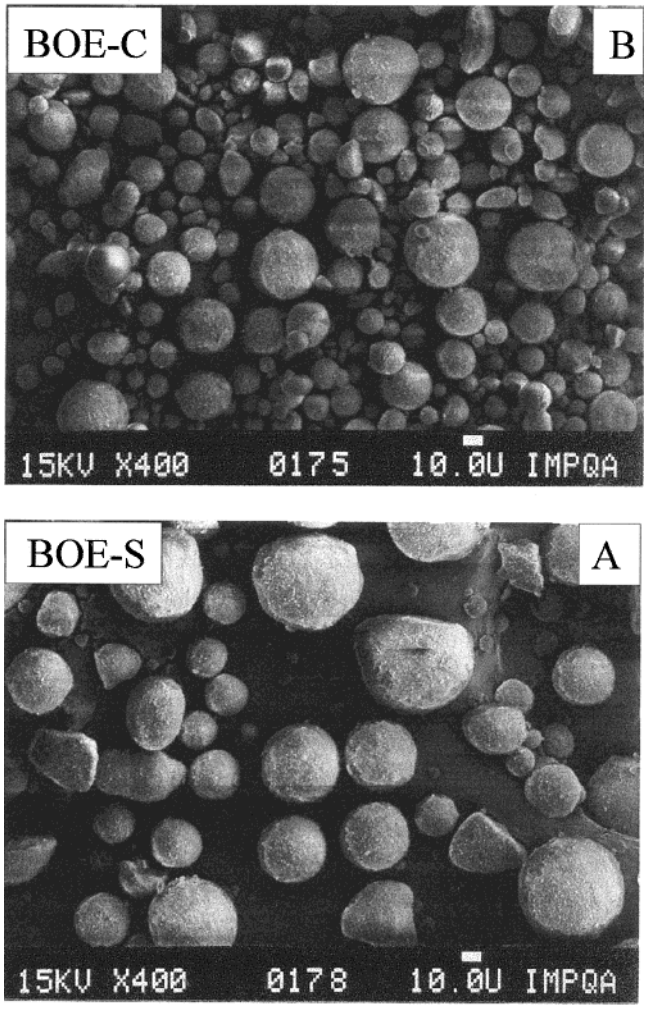

Figure 8. Scanning electron micrographs of annealed boehmite: (A) BOE-S and (B) BOE-C.

is present. The small pore size in these samples (Figure 14) gave rise to high specific areas and pore volumes (Table 7); the centroid of their distributions moved from 5 nm for PSB-C to around 11 nm when PSB was annealed under steaming conditions (Figure 14).

Although BOE-C and PSB-S had similar crystallite sizes, their adsorption loop hysteresis were very different (Figures 11 and 12). This shows that porosity is not determined by the alumina crystallite size but by its grain size. According to Scheme 1, alumina grains would be composed by a number of crystallites; this number decreases as the precursor crystallite size diminishes. Therefore, the grain size of transitional alumina derived from BOE would be larger than the one derived from PSB. A wider crystallite size distribution of PSB compared to BOE would create higher potential for crystal growth,[30] thus producing poorly ordered and less rigid structures possessing less strength.

Aluminas derived from BOE had smaller BET surface areas than those derived from PSB. This would be explained by the fact that crystallites in BOE were larger compared to crystallites in PSB. In both systems, however, steaming led to a decrease in surface area that is accompained by crystal growth (Table 7). The surface area was comparatively less affected in BOE-S, thus indicating a more stable phase that is related to a larger grain size.

Implications on the Properties of Transitional Aluminas as Potential Active Matrixes for Cracking Catalysts. Upon

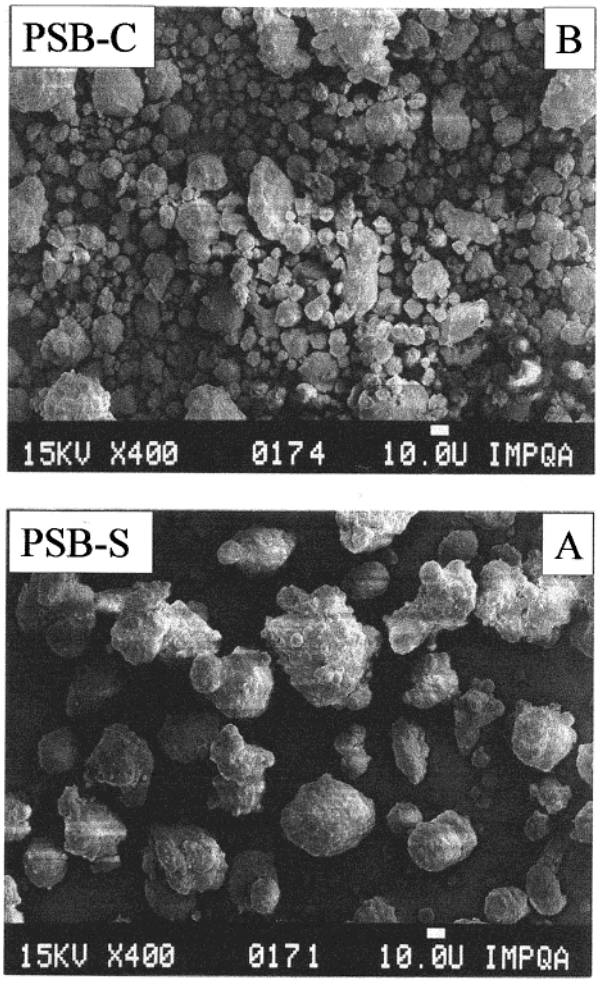

Figure 9. Scanning electron micrographs of annealed pseudoboehmite: (A) PSB-S and (B) PSB-C.

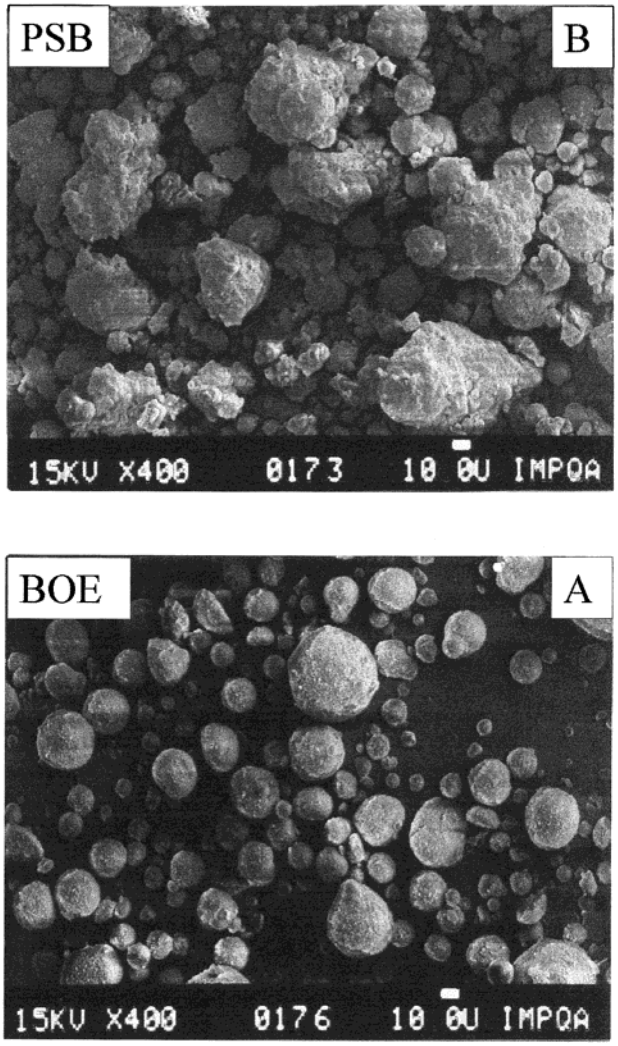

Figure 10. Precursors scanning electron micrographs: (A) BOE and (B) PSB.

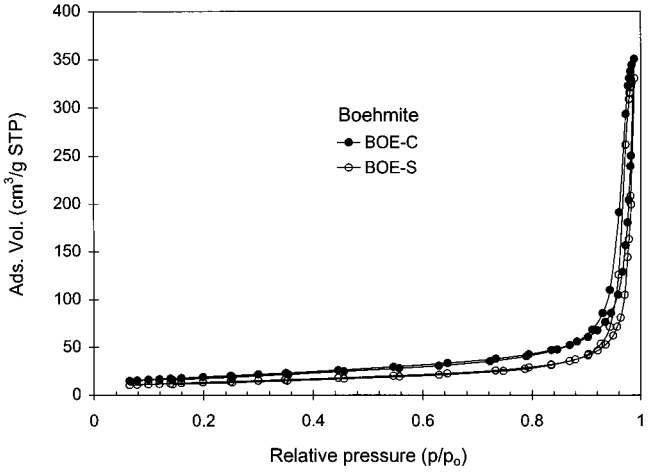

Figure 11. Nitrogen adsorption−desorption isotherms of BOE-C and BOE-S.

annealing, small crystallite boehmite produced transitional alumina possessing a less ordered structure and larger surface areas with smaller and irregular pores. Less hydrothermal stability, in terms of surface area loss and crystal growth, was also found. While this trend confirms what is already known, fundamental aspects based on structural considerations that explain such properties have been found in this work. The structural analysis of boehmite suggests that the surface of these solids will present different type of sites and that their relative population will depend on the crystallite size. From the bonds between aluminum and oxygen atoms (Table 6), it is observed that the bond lengths determining unit cell dimensions are different (Table 3), thus giving rise to different sites on the crystal faces perpendicular to the [100], [010], and [001] directions. Faces perpendicular to the [010] direction will contribute the most to surface properties in large crystallites, while faces perpendicular to [100] and [001] directions will have a considerable contribution in small crystallites. Transformation to transitional alumina is a pseudomorphic process, and therefore, these relative contributions will prevail in the annealed samples. On the other hand, as texture will depend on the crystallite ordering, less ordered surfaces will be obtained with materials possessing small crystallites. Implications from the catalytic standpoint concern more heterogeneous pore sizes and geometries found in aluminas derived from PSB.

Not only is the smaller pore size found in PSB derived aluminas less desirable for the cracking of large hydrocarbon molecules, but pore blockage would also produce less coke tolerance. In contrast, BOE aluminas have fewer acid sites which is a required property for cracking activity. It follows that a control of porosity is probably needed in the case of PSB derived aluminas, while increasing the number of active sites will probably improve the cracking activity of BOE aluminas.

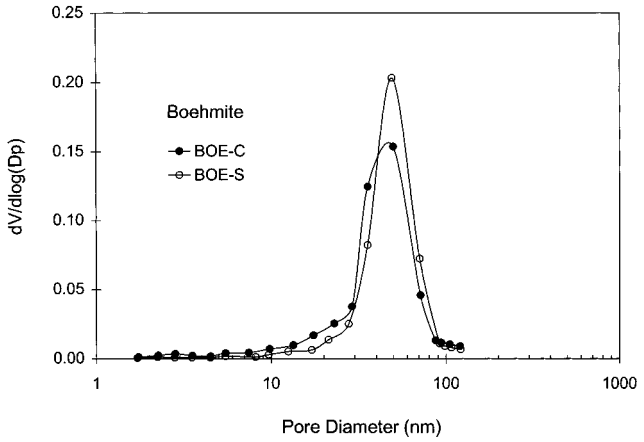

Figure 12. Pore size distribution of BOE-C and BOE-S.

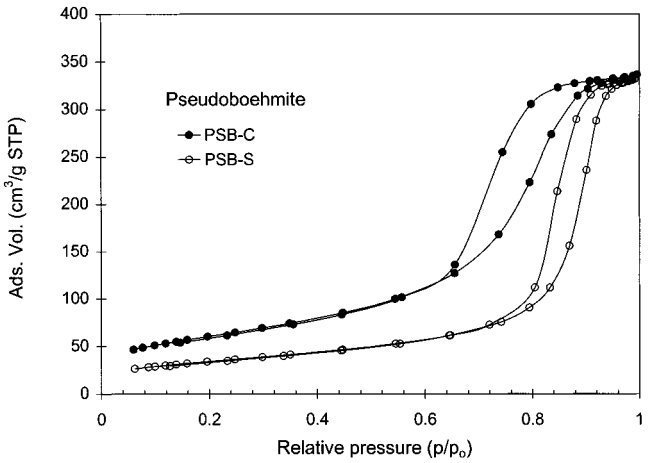

Figure 13. Nitrogen adsorption−desorption isotherms of PSB-C and PSB-S.

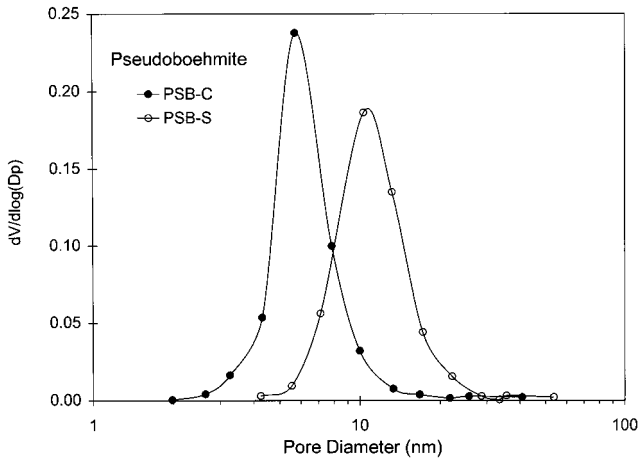

Figure 14. Pore size distribution of PSB-C and PSB-S.

TABLE 7: Textural Properties of the Transitional Aluminas

sample	specific area (m^2/g)	pore volume (cc/g)	average pore size (nm)
BOE-C	69.2	0.32	40.9
BOE-S	48.7	0.25	30.4
PSB-C	218.4	0.52	6.6
PSB-S	124.0	0.51	12.1

Conclusions

Using X-ray analysis and refinement techniques of the crystalline structures of boehmite and pseudoboehmite samples, the same crystalline structure was observed. The lattice parameters and atom positions in the unit cell were similar. However, differences in crystallite size were determined, with pseudoboehmite having shown smaller crystallite size. The largest structural difference was observed for the *b* axis magnitude. The calculated value of 0.0052 nm is not enough to assume that pseudoboehmite would have intercalated water in its crystalline structure. The higher water content always observed for pseudoboehmite compared to boehmite during drying should be ascribed to crystallites with larger active areas and associated with water molecules adsorbed in faces perpendicular to (020) planes. The transition temperature of boehmite into transitional alumina depended on the hydrogen bond between boehmite double-octahedra layers. Boehmite crystallite dimensions also defined pore size and distribution of the transitional alumina as well as its crystallite size. Since the transformation of transitional alumina into α-Al_2O_3 depends on the diffusion of hydroxyls, the temperature associated with structural transformation is higher for transitional alumina with a larger grain size. Annealing under steaming conditions hindered formation of small crystallite agglomerates and gave rise to transitional aluminas with larger crystallites, because it favored transporting of aluminum atoms; this effect was larger for pseudoboehmite. Nitrogen adsorption−desorption isotherms showed that in the transitional alumina derived from pseudoboehmite, platelet-like grains were less ordered with water intercalated between the platelets.

Consequences on the properties of transitional aluminas used as cracking catalysts were inferred. As texture and acidity evolve in opposite directions, there is a need for controlling them independently. A deeper comprehension on the origin of these properties will certainly help to reach this goal.

Acknowledgment. We would like to thank Mr. A. Morales and Mr. M. Aguilar for technical assistance; we also tank Mr. B. Handy for his help in reviewing the manuscript. This work was financially supported by IMP projects D.01024 and D.01234

References and Notes

(1) Ismagilov, Z. R.; Shkrabina, R. A.; Koryabkina, N. A. *Catal. Today* **1999**, *47*, 51.
(2) Hietala, J.; Root, A. R.; Knuutila, P. *J. Catal.* **1994**, *150*, 46.
(3) Barath, F.; Turki, M.; Keller V.; Maire, G. *J. Catal.* **1999** *185*, 1.
(4) Grange, P. *Catal. Rev.- Sci.- Eng.* **1980**, *21*, 135.
(5) Lerner, B. A. US Patent 5,559,067, 1996, assignee Engelhard Corp.
(6) O'Connor, P.; Verlaan, J. P. J.; Yanik, S. J. *Catal. Today* **1998**, *43*, 305.
(7) Cheng, W.-Ch.; Rajagopalan, K. US Patent 5,547564, 1996, assignee W. R. Grace & Co.-Conn.
(8) Lussier, R. J. US Patent 4,894,143, 1990, assignee W. R. Grace & Co.-Conn.
(9) Upson, L.; Van de Gender, P. J.; Van Dijk, W. US Patent 5,173,-174, 1992, assignee UOP
(10) Otterstedt, J. E.; Gevert, S. B.; Jaras, S. G.; Menon, P. G. *Appl. Catal.* **1988**, *38*, 143.
(11) O'Connor, P.; Gevers, A. W.; Humpries, A.; Gerrisen, L. A.; Desai, P. H. In *Fluid Catalytic Cracking II: Concepts in Catalyst Design;* Occelli, M., Ed.; ACS Symposium Ser. 452; American Chemical Society: Washington, DC, 1991; p 318.
(12) Woolery, G. L.; Farnos, M. D.; Quinones, A. R.; Chin, A. In *Fluid Cracking Catalysts*; Occelli, M. L., O'Connor, P., Eds.; Marcel Dekker: New York, 1998; Vol. 74, p 48.
(13) Alearasool, S.; Doolin, P. K.; Hoffman, J. F. In *Fluid Cracking Catalysts*; Occelli, M. L., O'Connor, P., Eds.; Marcel Dekker: New York, 1998; Vol. 74, p 96.
(14) Young, R. A.; Sakthivel, A.; Moss, T. S.; Paiva-Santos, C. O. *J. Appl. Crystallogr.* **1995**, *28*, 366.
(15) Rodríguez-Carbajal, J. Laboratoire Leon Brillouin (CEA-CNRS), France. Tel: (33) 1 6908 3343. Fax: (33) 1 6908 8261. E-mail: juan@llb.saclay.cea.fr.
(16) Thompson, P.; Cox, D. E.; Hasting, J. B. *J. Appl. Crystallogr.* **1987**, *20*, 79.
(17) Young R. A.; Desai, P. *Arch. Nauki Mater.* **1989**, *10*, 71.

(18) Prince, E. *J. Appl. Crystallogr.* **1981**, *14*, 157
(19) IUPAC, Manual of Symbols and Terminology for Physicochemical Quantities and Units; Appendix II, Definitions, terminology and symbols in colloid and surface chemistry; *Pure Appl. Chem.* **1972**, *31*, 578.
(20) Brunauer, S.; Emmett, P. H.; Teller, E. *J. Am. Chem. Soc.* **1938**, *60*, 309.
(21) Brunauer, S.; Demming, L. S.; Demming, W. E.; Teller, E. *J. Am. Chem. Soc.* **1940**, *62*, 1723.
(22) Salmones, J.; Garciafigueroa E.; Mayagoitia, V.; Rojas, F.; Kornhauser I. *Adsorption Science and Technology*; Multi-Sc Pub. Co. LTD.: UK, 1997; 15 N 9, p 661.
(23) Tsukada, T.; Segawa, H.; Yasumori, A.; Okada, K. *J. Mater. Chem.* **1999**, *9*, 549.
(24) Ismagilov, Z. R.; Shkrabina, R. A.; Koryabkina, N. A. *Catal. Today* **1999**, *47*, 51.
(25) Rodríguez-Carvajal, J.; Fernández, M. T.; Martínez, J. L. *J. Phys: Condens. Matter.* **1991**, *3*, 3215.
(26) Husson, E.; Repelin, Y. *Eur. J. Solid State Inor. Chem.* **1996**, *33*, 1223.
(27) Lippens, B. C.; de Boer, J. H. *Acta Crystallogr.* **1964**, *17*, 1312.
(28) Tikhov, S. F.; Fenelonov, V. B.; Zaikovskii, V. I.; Potapova, Yu. V.; Sadykov, V. A. *Microporous Mesoporous Mater.* **1999**, *33*, 137.
(29) Bokhimi, X.; Toledo-Antonio, J. A.; Guzmán-Castillo, M. L.; Hernández-Beltrán, F. *J. Solid State Chem.*, accepted.
(30) Mamchick, A. I.; Kalinin, S. V.; Vertegel, A. A. *Chem. Mater.* **1998**, *10*, 3548.
(31) Toledo-Antonio, J. A.; Bokhimi, X.; Guzmán-Castillo, M. L.; Mar-Mar, B.; Hernández-Beltrán, F. *Chem. Mater.* Submitted.
(32) Lippens, B. C.; Linsen, B. G.; De Boer, J. H. *J. Catal.* **1964**, *3*, 32.